molecules

MDPI

Article

A New Compartmentalized Scale (P_N) for Measuring Polarity Applied to Novel Ether-Functionalized Amino Acid Ionic Liquids

Xu Zheng, Chun Guo, Wenqing Wu and Jing Tong *

College of Chemistry, Liaoning University, Shenyang 110036, China; zhengxu120512@163.com (X.Z.); guochun654321@163.com (C.G.); wwq18435221725@163.com (W.W.)
* Correspondence: tongjinglnu@sina.com or tongjing@lnu.edu.cn

Abstract: Functionalized and environmentally friendly ionic liquids are required in many fields, but convenient methods for measuring their polarity are lacking. Two novel ether-functionalized amino acid ionic liquids, 1-(2-methoxyethyl)-3-methylimidazolium alanine ([C_1OC_2mim][Ala]) and 1-(2-ethoxyethyl)-3-methylimidazolium alanine ([C_2OC_2mim][Ala]), were synthesized by a neutralization method and their structures confirmed by NMR spectroscopy. Density, surface tension, and refractive index were determined using the standard addition method. The strength of intermolecular interactions within these ionic liquids was examined in terms of standard entropy, lattice energy, and association enthalpy. A new polarity scale, P_N, is now proposed, which divides polarity into two compartments: the surface and the body of the liquid. Surface tension is predicted via an improved Lorentz-Lorenz equation, and molar surface entropy is used to determine the polarity of the surface. This new P_N scale is based on easily measured physicochemical parameters, is validated against alternative polarity scales, and is applicable to both ionic and molecular liquids.

Keywords: polarity scale; ionic liquids; ether-functionalized; intermolecular interactions; molar surface entropy; Lorentz-Lorenz equation

Citation: Zheng, X.; Guo, C.; Wu, W.; Tong, J. A New Compartmentalized Scale (P_N) for Measuring Polarity Applied to Novel Ether-Functionalized Amino Acid Ionic Liquids. *Molecules* **2022**, *27*, 3231. https://doi.org/10.3390/molecules27103231

Academic Editor: Francesca D'Anna

Received: 23 April 2022
Accepted: 17 May 2022
Published: 18 May 2022

1. Introduction

The green chemistry concept is a widely accepted focus of modern chemical research, including the design of new materials. Ionic liquids (ILs) have emerged as useful green reaction media due to their many unique features, such as low vapor pressure and high thermal stability [1,2]. They play important roles in many fields, including energy storage [3], catalysis [4], pharmaceuticals, and medicine [5,6]. However, the relatively high viscosity of ILs is a barrier to further practical applications. Inserting ether groups into the cations of ILs has been shown to substantially reduce their viscosity without lowering thermal stability, while also reducing their toxicity [7–10]. Ether-functionalized ILs (EFILs) have demonstrated remarkable performance in many fields. For example, they dissolve lignocellulosic biomasses [7], reduce viscosity and provide coordination sites for lithium ions in Li/Li-ion batteries [8], and enhance CO_2 selectivity during CO_2 capture [11]. However, traditional ILs containing anions such as Cl^-, $[BF_4]^-$, and $[PF_6]^-$ are environmentally hazardous. The development of environmentally friendly, task-specific ILs based on renewable bioresources (such as amino acids and fatty acids) is an environmental necessity. Ohno and Fukumoto were the first to prepare amino acid ILs (AAILs), using 20 different amino acids as the anion; these AAILs demonstrated lower toxicity [12,13]. AAILs have now been utilized in enantioselective separation [14], extraction separation [15], and CO_2 capture [11]. ILs with imidazolium-based cations exhibit low toxicity. Meanwhile, the shorter the alkyl chain on the imidazole ring, the lower the toxicity [16,17]. Thus, imidazolium ILs have proved more attractive than ILs based on ammonium, phosphonium, and pyridinium cations. The

present study describes the preparation of two novel ether-functionalized, imidazolium-based AAILs: 1-(2-methoxyethyl)-3-methylimidazolium alanine ([C_1OC_2mim][Ala]) and 1-(2-ethoxyethyl)-face Tension, and Refractive Inde ([C_2OC_2mim][Ala]), together abbreviated as [$C_nOC_2$mim][Ala](n = 1, 2).

There is scope for considerable further research into EFILs because their physiochemical properties are highly susceptible to changes in structure. More experimental data are required to elucidate their structure–property relationships. This study measures the density, surface tension, and refractive index of [$C_nOC_2$mim][Ala](n = 1, 2). Density correlates with packing efficiency and intermolecular interactions and is a critical design property in chemical engineering [18]. Its study provides insight into the microstructure and macroscopic properties of ILs [19]. Surface tension is a crucial property at liquid–gas interfaces [20], affecting how the phases interact [21]. The surface tension of ILs is between those of alkanes and water [22]. It can be measured directly or predicted using, for example, the parachor formula [23] or group contribution methods [24]. This study predicts surface tension using an improved Lorentz-Lorenz equation. ILs are often used as solvents, so determining their polarity is crucial. Due to their non-structured nature, polarity cannot be determined by traditional methods such as relative permittivity (ε_r) and dipole moment (δ) [25]. The most widely used experimental method for IL polarity is the $E_T(30)$ scale, which measures the solvatochromic UV−Vis absorbance shift of a solute. However, this method is time-consuming and expensive, so attempts have been made to develop predictive models [26,27].

The present study proposes a new polarity scale, P_N, which enables polarity to be predicted from the easily measured physicochemical properties of density, surface tension, and refractive index. Following on from our previous studies [28–30], (i) [$C_nOC_2$mim][Ala] (n = 1, 2) are synthesized and their structures confirmed by nuclear magnetic resonance spectroscopy (NMR); (ii) their density, surface tension, and refractive index are measured from 288.15 to 328.15 K at 5 K intervals; (iii) the strength of their molecular interactions are studied based on standard entropy, lattice energy, and association enthalpy; (iv) an improved Lorentz-Lorenz equation is used to predict the surface tension of ILs and molecular liquids; and (v) a new scale, P_N, for estimating polarity is proposed, combining molar surface entropy s (which measures the polarity of the surface of a liquid) and the polarity coefficient P^2 (which measures the polarity of the body of a liquid).

2. Results and Discussion

2.1. Density, Surface Tension, and Refractive Index of [$C_nOC_2$mim][Ala](n = 1, 2)

The density (ρ), surface tension (γ), and refractive index (n_D) of [$C_nOC_2$mim][Ala] (n = 1, 2) with various water contents over 288.15–328.15 K (at 5 K intervals) are shown in Tables S1–S3 Supplementary Materials, with each value being an average of three measurements using the standard addition method. These parameters were plotted against water content (Figure 1), producing a series of straight lines with correlation coefficient squares (r^2) consistently greater than 0.99. The y-axis intercepts of these lines give the experimental value of each parameter in anhydrous [$C_nOC_2$mim][Ala](n = 1, 2) (Table 1).

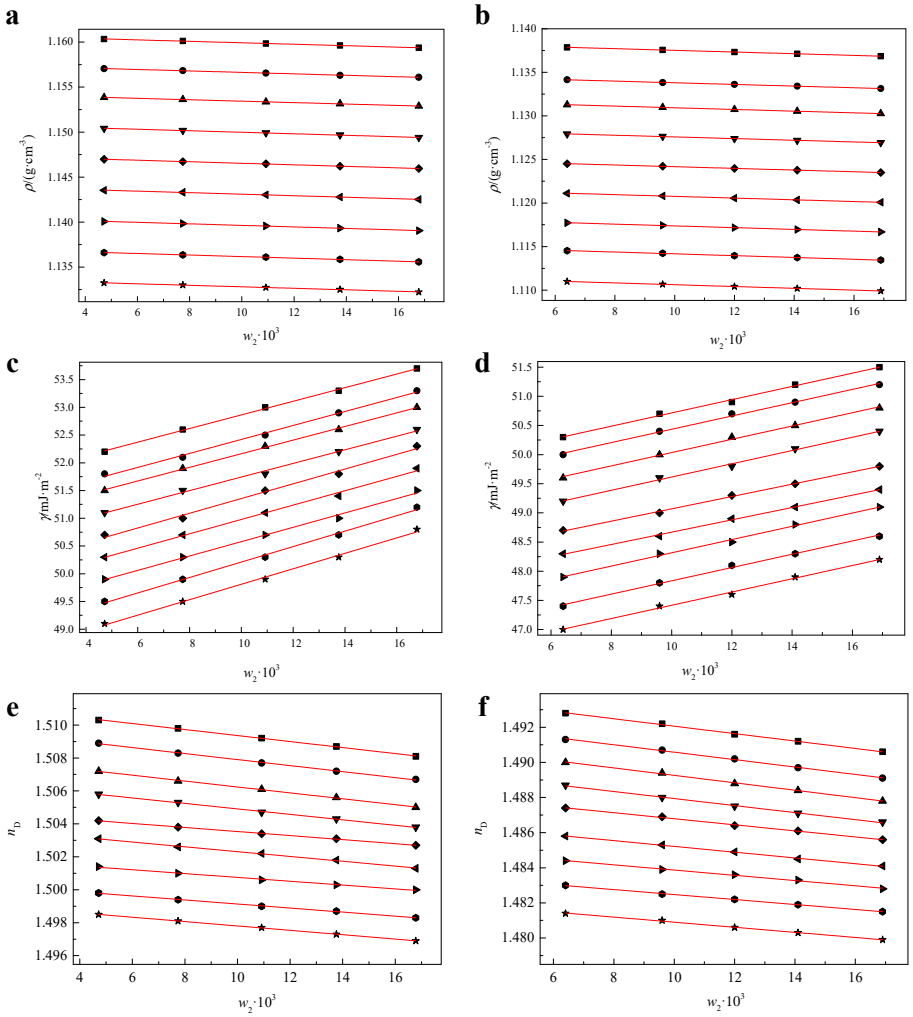

Figure 1. Density (ρ), surface tension (γ), and refractive index (n_D) plotted against water content (w_2) at various temperatures for [C_1OC_2mim][Ala] (**a**,**c**,**e**, respectively) and for [C_2OC_2mim][Ala] (**b**,**d**,**f**, respectively). ■ 288.15 K; ● 293.15 K; ▲ 298.15 K; ▼ 303.15 K; ◆ 308.15 K; ◀ 313.15 K; ▶ 318.15 K; ● 323.15 K; ★ 328.15 K.

Table 1. Density (ρ), surface tension (γ), refractive index (n_D), and thermal expansion coefficient (α) at various temperatures (T) for [$C_nOC_2$mim][Ala](n = 1, 2).

T (K)	ρ (g·cm^{-3})	γ (mJ·m^{-2})	n_D	α (K^{-1} × 10^4)
		[C_1OC_2mim][Ala]		
288.15	1.16073	51.6	1.5112	5.8555
293.15	1.15744	51.2	1.5097	5.8722
298.15	1.15423	50.9	1.5080	5.8885
303.15	1.15082	50.5	1.5066	5.9060
308.15	1.14739	50.0	1.5048	5.9236
313.15	1.14395	49.7	1.5038	5.9414
318.15	1.14049	49.3	1.5019	5.9595
323.15	1.13703	48.8	1.5004	5.9776
328.15	1.13365	48.4	1.4991	5.9954

Table 1. *Cont.*

T (K)	ρ (g·cm^{-3})	γ (mJ·m^{-2})	n_D	α (K^{-1} × 10^4)
		[C_2OC_2mim][Ala]		
288.15	1.13849	49.6	1.4942	5.8490
293.15	1.13475	49.3	1.4927	5.8683
298.15	1.13190	48.9	1.4914	5.8830
303.15	1.12854	48.5	1.4899	5.9005
308.15	1.12514	48.0	1.4885	5.9184
313.15	1.12175	47.6	1.4869	5.9363
318.15	1.11838	47.2	1.4854	5.9541
323.15	1.11521	46.7	1.4839	5.9711
328.15	1.11166	46.3	1.4824	5.9901

Standard uncertainties (u) are $u(T)$ = 0.02 K and $u(p)$ = 10 kPa; expanded uncertainties (U) are $U(\rho)$ = 0.002 g·cm^{-3}, $U(\gamma)$ = 0.3 mJ·m^{-2}, and $U(n_D)$ = 0.003, with 95% confidence (k = 2).

2.2. Strength of [$C_nOC_2$mim][Ala](n = 1, 2) Intermolecular Interactions

The density of ILs increases gradually as temperature rises. At higher temperatures, the mobility of constituent ions improves and the unit volume increases [31]. The thermal expansion coefficient (α) is defined as

$$\alpha = (1/V)(\partial V/\partial Y)_p = -(\partial\, ln\rho/\partial T)_p \quad (1)$$

where V is molar volume. Molar volume is defined as

$$V = \mathrm{M}/\rho \quad (2)$$

The molecular volume V_m is defined as

$$V\mathrm{m} = \mathrm{M}/\mathrm{N}\rho = V/\mathrm{N} \quad (3)$$

where N is the Avogadro constant, V is molar volume, and M is molar mass.

At 298.15 K, V_m is 0.3300 nm^3 for [C_1OC_2mim][Ala] and 0.3571 nm^3 for [C_2OC_2mim][Ala] (Table S4). The difference between these indicates that the contribution of methylene (-CH_2-) to V_m is 0.0271 nm^3. This is close to the average contribution methylene makes to the V_m of several other ILs listed in Table S5 (0.0278 nm^3).

Lattice energy (U_{POT}) and standard entropy ($S^{\theta}{}_{298}$) can be calculated according to Glasser's theory; Equation (4) is suitable for MX(1:1) type ionic salts. The constants in Equation (5) are empirical values [32].

$$U_{POT} = 1981.2\ (\rho/\mathrm{M})^{1/3} + 103.8 \quad (4)$$

$$S^{\theta}{}_{298} = 1246.5V\mathrm{m} + 29.5 \quad (5)$$

U_{POT} reflects the strength of intermolecular interactions and can be used to measure the stability of ILs [32,33]. U_{POT} is 443 kJ·mol^{-1} for [C_1OC_2mim][Ala] and 435 kJ·mol^{-1} for [C_2OC_2mim][Ala], implying that methylene's average contribution to U_{POT} is −8 kJ·mol^{-1}. U_{POT} is inversely related to molar volume. Addition of a methylene group will reduce the ionic or molecular packing efficiency, decreasing the strength of the interactions.

To some extent, standard entropy reflects the degree of disorder of molecular arrangements [33]. $S^{\theta}{}_{298}$ is 441 J·K^{-1}·mol^{-1} for [C_1OC_2mim][Ala] and 475 J·K^{-1}·mol^{-1} for [C_2OC_2mim][Ala], suggesting that methylene's average contribution to $S^{\theta}{}_{298}$ is 34 J·K^{-1}·mol^{-1} (Table S5). This indicates that ILs with longer aliphatic chains are more disordered. Standard entropy increases as molecular volume increases. $S^{\theta}{}_{298}$ of ILs is usually greater than 200 J·K^{-1}·mol^{-1}, compared with the more molecularly ordered conventional inorganic salts such as NaCl (72.1 J·K^{-1}·mol^{-1}) and KCl (82.6 J·K^{-1}·mol^{-1}) [34]. This may explain why ILs are molten below 373 K.

The association enthalpy ($\Delta_A H_m{}^0$) also reflects the strength of intermolecular interactions: the higher the $\Delta_A H_m{}^0$, the stronger the gaseous state interactions. $\Delta_A H_m{}^0$ of ILs in the gaseous phase can be calculated based on the thermodynamic cycle shown in Scheme 1 [29].

$$M^+(g) + X^-(g) \rightarrow [MX]^0(g)$$
$$\uparrow \qquad\qquad \uparrow$$
$$\text{[Liquid state ILs, MX]}$$

Scheme 1. Thermodynamic cycle for calculating $\Delta_A H_m{}^0$.

Vaporization enthalpy ($\Delta_l{}^g H_m{}^0$) is a key parameter for calculating $\Delta_A H_m{}^0$. It is estimated from Equation (6):

$$g_s = a + b\left(\Delta_l{}^g H_m{}^0 - RT\right) \quad (6)$$

$$g_s = \gamma V^{2/3} N^{1/3} \quad (7)$$

where g_s is the molar surface Gibbs energy; γ is surface tension; V is molar volume; N is the Avogadro constant; $\Delta_l{}^g H_m{}^0$ is vaporization enthalpy; R is the gas constant; T is temperature; and a and b are the empirical constants -1.519 kJ·mol^{-1} and 0.09991, respectively [29].

The estimated vaporization enthalpy is 164.1 kJ·mol^{-1} for [C_1OC_2mim][Ala] and 165.1 kJ·mol^{-1} for [C_2OC_2mim][Ala]. Consequently, $\Delta_A H_m{}^0$ is -278.9 kJ·mol^{-1} for [C_1OC_2mim][Ala] and -269.9 kJ·mol^{-1} for [C_2OC_2mim][Ala]. The $\Delta_A H_m{}^0$ of other ILs are listed in Table S5. Again, addition of methylene reduces packing efficiency and increases the degree of molecular disorder. Thus, for ILs with the same anions, the absolute value of $\Delta_A H_m{}^0$ decreases as the length of the imidazole ring alkyl side chains increases. For ILs with the same cations, $\Delta_A H_m{}^0$ decreases with increasing anion volume.

2.3. Prediction of Surface Tension Based on Molar Surface Gibbs Energy

The parameter g_s used to estimate vaporization enthalpy was developed in our previous work by modifying Li's model [35]. The definition of g_s is consistent with the concept presented by Myers [36]. Thus, g_s is a true thermodynamic function that integrates volumetric and surface properties.

Plotting g_s against T for [$C_nOC_2$mim][Ala](n = 1, 2) yields straight lines (Figure 2) such that their relationship can be expressed as

$$g_s = G_0 - G_1 T \quad (8)$$

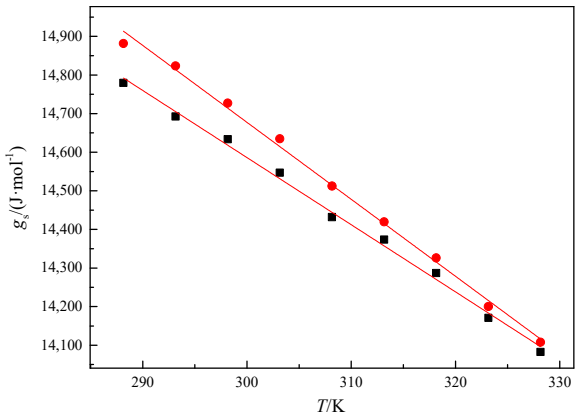

Figure 2. Molar surface Gibbs energy (g_s) plotted against temperature (T). ■ [C_1OC_2mim][Ala]: g_s = 19,803 − 17.39T, r^2 = 0.995, sd = 16.4; ● [C_2OC_2mim][Ala]: g_s = 20,658 − 19.94T, r^2 = 0.996, sd = 17.5.

G_0 and G_1 for [C_nOC$_2$mim][Ala](n = 1, 2) are obtained from Figure 2 and substituted into Equation (8) to give the estimated molar surface Gibbs energy, $g_{s(est)}$. Values of g_s, G_0, G_1, and $g_{s(est)}$ are listed in Table 2.

Table 2. Molar surface Gibbs energy (g_s), G_0, G_1, and estimated molar surface Gibbs energy ($g_{s(est)}$) for [C_nOC$_2$mim][Ala](n = 1, 2).

T (K)	g_s (kJ·mol^{-1})	G_0	G_1	$g_{s(est)}$ (kJ·mol^{-1})
		[C$_1$OC$_2$mim][Ala]		
288.15	14.78	19,803	17.4	14.79
293.15	14.69	19,803	17.4	14.70
298.15	14.63	19,803	17.4	14.62
303.15	14.55	19,803	17.4	14.53
308.15	14.43	19,803	17.4	14.44
313.15	14.37	19,803	17.4	14.35
318.15	14.29	19,803	17.4	14.27
323.15	14.17	19,803	17.4	14.18
328.15	14.08	19,803	17.4	14.09
		[C$_2$OC$_2$mim][Ala]		
288.15	14.88	20,658	19.9	14.92
293.15	14.82	20,658	19.9	14.82
298.15	14.73	20,658	19.9	14.72
303.15	14.63	20,658	19.9	14.63
308.15	14.51	20,658	19.9	14.53
313.15	14.42	20,658	19.9	14.43
318.15	14.33	20,658	19.9	14.33
323.15	14.20	20,658	19.9	14.23
328.15	14.11	20,658	19.9	14.13

The Lorentz-Lorenz equation expresses the relationship between n_D and the mean molecular polarizability (α_p) [37]:

$$R_m = [({n_D}^2 - 1)/({n_D}^2 + 2)] \cdot V = (4\pi N/3) \cdot \alpha_p \quad (9)$$

where R_m is molar refraction, α_p is mean molecular polarizability, and n_D is refractive index. This has been combined with g_s to give an improved Lorentz-Lorenz equation [38] that can predict surface tension, $\gamma_{(est)}$:

$${\gamma_{(est)}}^{3/2} = [{g_{s(est)}}^{3/2}/N^{1/2}R_m]({n_D}^2 - 1)/({n_D}^2 + 2) \quad (10)$$

The R_m, α_p, and $\gamma_{(est)}$ for [C_nOC$_2$mim][Ala](n = 1, 2) are listed in Table 3. Plotting estimated surface tension values against their corresponding experimental values produces a straight line (Figure 3). A similar plot for other ionic and molecular liquids also illustrates a linear relationship (Table S6, Figure 4), showing that this method is applicable for the surface tension prediction of both types of liquid.

Table 3. Molar refraction (R_m), mean molecular polarizability (α_p), and estimated surface tension ($\gamma_{(est)}$) of [C_nOC$_2$mim][Ala](n = 1, 2).

T (K)	Rm	$\alpha_p \times 10^{24}$	$\gamma_{(est)}$
	[C_1OC$_2$mim][Ala]		
288.15	57.74	22.91	51.6
293.15	57.77	22.92	51.2
298.15	57.76	22.92	50.8
303.15	57.80	22.93	50.4
308.15	57.82	22.94	50.0
313.15	57.84	22.95	49.6
318.15	57.89	22.97	49.2
323.15	57.90	22.97	48.8
328.15	57.89	22.97	48.4
	[C_2OC$_2$mim][Ala]		
288.15	62.24	24.69	49.4
293.15	62.28	24.71	49.0
298.15	62.30	24.72	48.6
303.15	62.32	24.73	48.2
308.15	62.36	24.74	47.7
313.15	62.37	24.75	47.3
318.15	62.39	24.76	46.9
323.15	62.41	24.76	46.5
328.15	62.43	24.77	46.1

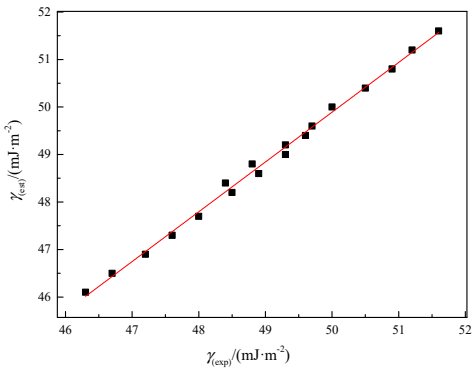

Figure 3. Plot of surface tension $\gamma_{(est)}$ against $\gamma_{(exp)}$ for [C_nOC$_2$mim][Ala](n = 1, 2). $\gamma_{(est)}$ =1.0581$\gamma_{(exp)}$ − 2.9851; r^2 = 0.995; sd = 0.11.

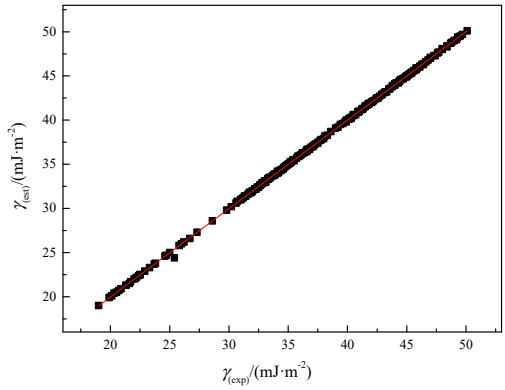

Figure 4. Plot of surface tension $\gamma_{(est)}$ against $\gamma_{(exp)}$ for various ionic and molecular liquids (see Table S6). $\gamma_{(est)}$ = 1.0009$\gamma_{(exp)}$ − 0.03643; r^2 = 0.999; sd = 0.10.

For ILs sharing the same anions (Table 1 and Table S6), n_D decreases as the length of the alkyl chain in the cations increases. Refractive index correlates with dipole moment [39,40],

which increases with higher molecular packing density [41]. Thus, a larger dipole moment results in a higher refractive index. The n_D is larger in $[C_1OC_2mim][Ala]$ than $[C_2OC_2mim][Ala]$, so the packing density of the former is higher, which is consistent with the density trend of the two ILs.

As polarizability increases, Coulomb interactions are reduced and ion mobility rises [42]. The α_p of $[C_1OC_2mim][Ala]$ is lower than $[C_2OC_2mim][Ala]$, so its Coulomb interactions are stronger. This finding is similar to the pattern observed for U_{POT} and $\Delta_A H_m{}^0$.

2.4. Molar Surface Entropy: Polarity Contribution from Surface Liquid

For most liquids, surface tension declines as temperature increases, as shown by the Eötvös equation:

$$\gamma V^{2/3} = k(Tc - T) \tag{11}$$

where T_c is critical temperature and k is the Eötvös equation parameter, which is associated with polarity. For some organic liquids with weak polarity, k is nearly 2.2×10^{-7} J·mol$^{-2/3}$·K^{-1}, while for some with strong polarity, such as molten NaCl, it is nearly 0.4×10^{-7} J·mol$^{-2/3}$·K^{-1} [35,43]. However, the physical significance of k is not clear. Multiplying both sides of the Eötvös equation by $N^{1/3}$ [35] gives

$$g_s = C_0 - C_1 T \tag{12}$$

which fits the fundamental thermodynamic concept:

$$G = H - TS \tag{13}$$

C_1 denotes the molar surface entropy and is given by $C_1 = -(\frac{\partial g_s}{\partial T})_p$.

The relationship between molar surface entropy (defined here as s [29]) and k is expressed as

$$s = N^{1/3} k \tag{14}$$

Entropy is directly linked to the number of microstates [44]. Higher entropy means molecules can be arranged in more ways, while the total energy remains constant. Thus, the physical significance of s is clear—it reflects the polarity of a liquid's surface (higher s, lower surface polarity). The value of s is 17.39 J·mol^{-1}·K^{-1} for $[C_1OC_2mim][Ala]$ and 19.94 J·mol^{-1}·K^{-1} for $[C_2OC_2mim][Ala]$. Values for other EFILs are listed in Table 4. The overall trend is that for ILs with the same cations, such as $[C_1OC_2mim]^+$, $[C_2OC_2mim]^+$, and $[C_1OC_4mim]^+$, s increases as the volume of anions increases. Cl^-, $[Ala]^-$, $[Thr]^-$, and $[Gly]^-$ clearly obey this rule. It can be speculated that larger anions cause greater disordering of surface molecules, leading to lower polarity. However, $[NTf_2]^-$ does not conform to this rule. This may be due to it being more symmetrical than other anions, facilitating a more orderly arrangement of surface molecules and increasing the polarity. For ILs sharing the same anions, the general trend is that s increases as the volume of cations increases. Values of s for different other ILs (Table S7) confirm this effect.

Table 4. Molar surface entropy (s) of various EFILs.

IL	s (J·mol^{-1}·K^{-1})	V × 10^4 (m^3·mol^{-1})
$[C_1OC_2mim]Cl$ [38]	15.99	1.52
$[C_1OC_2mim][Ala]$	17.39	1.99
$[C_1OC_2mim][Thr]$ [45]	26.60	2.18
$[C_1OC_2mim][NTf_2]$ [19]	17.80	2.80
$[C_2OC_2mim]Cl$ [38]	17.81	1.68
$[C_2OC_2mim][Ala]$	19.94	2.15
$[C_2OC_2mim][Thr]$ [45]	28.12	2.37
$[C_2OC_2mim][NTf_2]$ [19]	19.32	2.99
$[C_1OC_4mim][Gly]$ [46]	19.56	2.19
$[C_1OC_4mim][Ala]$ [46]	20.54	2.29
$[C_1OC_4mim][Thr]$ [46]	22.082	2.51
$[C_2OC_1mim][NTf_2]$ [19]	18.20	2.81
$[C_1OC_3mim][NTf_2]$ [19]	18.49	2.97
$[C_3OC_2mim][NTf_2]$ [19]	20.57	3.16

Data for [C_1OC_2mim][NTf_2], [C_2OC_1mim][NTf_2], [C_2OC_2mim][NTf_2], and [C_1OC_3mim][NTf_2] (Table 4) imply that, for ILs with the same number of alkyl side chain carbons, the position of the ether group also affects *s*, presumably because it affects packing efficiency on the liquid surface.

2.5. A New Model for Predicting Polarity

Experimental methods for measuring polarity, such as $E_T(30)$, are time consuming and laborious. Here, we present a predictive model that establishes a relationship between polarity and the easily determined physicochemical properties of density, surface tension, and refractive index.

Our previous work [28], based on Hildebrand and Scott's theory [47], proposed δ_μ as a polarity scale. δ_μ is the solubility parameter derived from the contribution of the average permanent dipole moment:

$$\delta_\mu{}^2 = \Delta^g{}_lH^0{}_{m\mu}/V - (1 - x)RT/V \quad (15)$$

where V is the molar volume and $\Delta^g{}_lH^0{}_{m\mu}$ is the contribution of the average permanent dipole moment to $\Delta^g{}_lH^0{}_m$, such that

$$\Delta^g{}_lH^0{}_{m\mu} = \Delta^g{}_lH^0{}_m - \Delta^g{}_lH^0{}_{mn} \quad (16)$$

where $\Delta^g{}_lH^0{}_{mn}$ is the contribution of the induced dipole moment to $\Delta^g{}_lH^0{}_m$ and can be calculated from the Lawson–Ingham equation [48]:

$$\Delta^g{}_lH^0{}_{mn} = C\,[(n_D{}^2 - 1)\,/\,(n_D{}^2 + 2)]V = C\,Rm \quad (17)$$

where C is the empirical constant 1.297 $kJ{\cdot}cm^{-3}$. In Equation (15), x represents $\Delta^g{}_lH^0{}_{mn}/\Delta^g{}_lH^0{}_m$ (at 298.15 K). The δ_μ polarity of [C_1OC_2mim][Ala] (21.03 $J^{1/2}{\cdot}cm^{-3/2}$) is larger than [C_2OC_2mim][Ala] (19.65 $J^{1/2}{\cdot}cm^{-3/2}$).

However, there is an obvious drawback to δ_μ: it has a dimension ($J^{1/2}{\cdot}cm^{-3/2}$), while some polarity scales, such as the dielectric constant, are non-dimensional. Furthermore, the contribution of the induced dipole moment was neglected. Therefore, δ_μ was improved as follows and designated as P [45]:

$$P = \delta_\mu/\delta_n = \left[\left(\Delta^g{}_lH^0{}_{m\mu}/V - (1-x)\,RT/V\right)/\left(\Delta^g{}_lH^0{}_{mn}/V - xRT/V\right)\right]^{1/2} \quad (18)$$

where δ_n is the solubility parameter from the contribution of the induced dipole moment. Comparison of $\Delta^g{}_lH^0{}_{m\mu}$ and $\Delta^g{}_lH^0{}_{mn}$ shows that $(1-x)RT/V$ and xRT/V can be omitted and Equation (18) can be expressed as

$$P = \left(\Delta^g{}_lH^0{}_{m\mu}/\Delta^g{}_lH^0{}_{mn}\right)^{1/2} \quad (19)$$

The effects of average permanent dipole moment and induced dipole moment are both considered within P, which is dimensionless, with a large value indicating high polarity. [C_4mim][BF_4] is hydrophilic and [C_4mim][NTf_2] is hydrophobic. According to Seddon et al. [49], P is 1.226 for [C_4mim][BF_4] and 0.401 for [C_4mim][NTf_2]. This higher polarity of [C_4mim][BF_4] fits practical experience. Thus, the parameter P is capable of measuring the polarity of ILs. P is 1.191 for [C_1OC_2mim][Ala] and 1.043 for [C_2OC_2mim][Ala].

This study divided polarity into two compartments: the contribution from the body of a liquid, and the contribution from the surface. Cohesive energy density can demonstrate the strength of intermolecular interactions within the body [48]. ${\delta_\mu}^2$ is the cohesive energy density from the average permanent dipole moment and ${\delta_n}^2$ is from the induced dipole moment. Consequently, P^2 can describe the polarity of the body of a liquid:

$$P^2 = {\delta_\mu}^2/{\delta_n}^2 \tag{20}$$

Molar surface entropy (s) was proven above to reflect the polarity of a liquid surface. Combining s and P^2, a new polarity scale, P_N, is now proposed:

$$P_N = s/P^2 = s/\left({\delta_\mu}^2/{\delta_n}^2\right) \tag{21}$$

This compartmentalized scale is a novel method to evaluate polarity, with a large P_N indicating weak polarity. Based on literature data [50–55], P_N is 22.03 $J{\cdot}mol^{-1}{\cdot}K^{-1}$ for $[C_4mim][NTf_2]$ and 14.50 $J{\cdot}mol^{-1}{\cdot}K^{-1}$ for $[C_4mim][BF_4]$. These results fit with practical experience and demonstrate the rationality of the P_N scale. The P_N of $[C_1OC_2mim][Ala]$ is 12.26 $J{\cdot}mol^{-1}{\cdot}K^{-1}$ and is 18.33 $J{\cdot}mol^{-1}{\cdot}K^{-1}$ for $[C_2OC_2mim][Ala]$, which is the same polarity trend observed using δ_μ and P. As discussed above, ILs with longer alkyl chains exhibit higher standard entropy and lower molecular packing efficiency. The observed higher polarity of $[C_1OC_2mim][Ala]$ may be due to its stronger intermolecular interactions and more ordered molecular arrangement. This fact can be explained as follows: a polar molecule has a permanent electric dipole moment, and a molecule may be polar if it has low symmetry [44]. ILs have asymmetric structures, and an orderly arrangement of ILs will maintain this structure. In this situation, their permanent electric dipole moments will not counteract each other, and polarity will be enhanced. The P_N of various ether-functionalized ILs are listed in Table 5. For ILs with the same anion, P_N declines as the length of the imidazole ring alkyl side chain increases. This trend supports the contention that the strength of intermolecular interactions and the degree of disorder of molecular arrangements influence polarity.

Table 5. Polarity of various ether-functionalized ionic liquids using the new P_N scale.

IL	P_N ($J{\cdot}mol^{-1}{\cdot}K^{-1}$)	Reference
$[COC_2mim]Cl$	12.86	[37]
$[C_2OC_2mim]Cl$	16.76	[37]
$[C_1OC_2mim][Ala]$	12.26	This work
$[C_2OC_2mim][Ala]$	18.33	This work
$[COC_4mim][Ala]$	21.83	[39]
$[COC_2mim][Thr]$	22.18	[38]
$[C_2OC_2mim][Thr]$	25.46	[38]
$[COC_4mim][Thr]$	24.52	[39]
$[COC_2mim][NTf_2]$	31.31	[13]
$[C_2OCmim][NTf_2]$	35.40	[13]
$[C_1OC_3mim][NTf_2]$	35.57	[13]
$[C_2OC_2mim][NTf_2]$	42.66	[13]
$[C_3OC_2mim][NTf_2]$	55.1	[13]
$[COC_4mim][Gly]$	19.64	[39]

The P_N scale can be validated by comparison with other polarity scales (Table 6). FTIR spectroscopy probes [56] and ${E_T}^N$ [57] show that the polarity of $[C_2mim]BF_4$ is larger than $[C_4mim]BF_4$. The P_N scale gives the same qualitative result. Wu et al. determined the order of polarity of several ILs to be $[C_4mim]BF_4 > [C_4mim]NTf_2 > [C_4mim]OAc$ using ${E_T}^N$ [58]. Again, P_N gives the same result.

Table 6. Polarity of various ionic liquids estimated using the P_N scale.

IL	P_N (J·mol^{-1}·K^{-1})
[C_6mim]OAC	35.73
[C_4mim]OAC	23.24
[C_4mim]NTf_2 [51,53]	22.03
[C_4mmim]NTf_2	19.96
[C_4mim]BF_4	14.50
[C_2mmim]NTf_2	14.01
[C_5mim]Lact	12.87
[C_2mim]BF_4	8.24
[C_2mim]Lact	8.16

Furthermore, when P_N is applied to molecular liquids, the estimated polarity is broadly, and inversely, consistent with the dielectric constant ε [59] (Table 7). The correlation between P_N and the inverse ε^{-1} (Figure 5) is $r^2 = 0.94$, demonstrating that P_N is also suitable for molecular liquids.

Table 7. P_N and dielectric constant (ε) of various molecular liquids.

Molecular Liquid	P_N	ε
Ethyl acetate	169.14	6.1
Chloroform	167.19	4.8
Tetrahydrofuran	124.29	7.5
Pyridine	60.64	12.3
Benzyl alcohol	48.13	13.0
1-Hexanol	27.06	13.0
Cyclohexanol	25.09	15.0
1-Propanol	8.48	20.3
Ethanol	5.52	25.3
Methanol	2.40	33.0

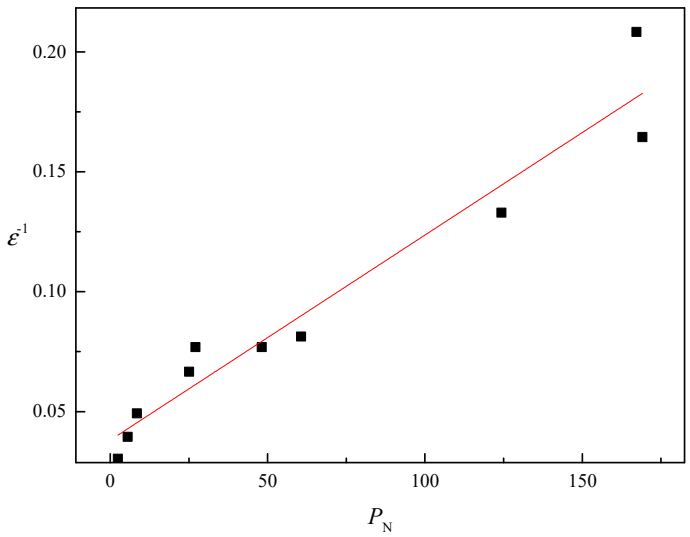

Figure 5. Inverse of the dielectric constant (ε^{-1}) of various molecular liquids plotted against the estimated polarity P_N. Linear correlation coefficient (r^2) 0.94.

$E_T(30)$ is one of the most popular polarity scales for evaluating ILs, but it is laborious and costly [60]. Moreover, the results vary depending on the molecular probe used [61]. However, using P_N, polarity can be determined simply from density, surface tension, and refractive index. The dielectric constant is the traditional polarity scale for organic solvents. The comparison of dielectric constant and P_N proves the universal applicability of P_N. Thus, this new P_N scale is demonstrated to be a viable predictive method for evaluating the polarity of both ionic and molecular liquids based on easily measured physicochemical properties. It will find applications in many fields, particular those employing novel ionic liquids for which the evaluation of polarity is expensive and time consuming.

3. Materials and Methods

3.1. Materials

The sources and purity of reagents are listed in Table 8. *N*-Methylimidazole (AR grade) was purified by distillation, while 2-chloroethyl methyl ether and 2-chloroethyl ethyl ether (both AR grade) were used as purchased. DL-Alanine was recrystallized from water and dried in a vacuum oven [62].

Table 8. Source and purity of reagents.

Reagent Name	CAS No.	Source	Purification	Mass Fraction Purity	Analysis
Anion exchange resin 717	122560-63-8	SRC	None	Granularity > 0.950	GC
N-Methylimidazole	616-47-7	ACROS	Distillation	>0.990	FM
2-Chloroethyl methyl ether	627-42-9	SRC	None	>0.995	FM
2-Chloroethyl ethyl ether	628-34-2	SRC	None	>0.995	FM
DL-Alanine	302-72-7	SRC	Recrystallization	>0.990	FM
Acetonitrile	75-05-8	SRC	None	>0.995	FM
Ethyl acetate	141-78-6	SRC	None	>0.995	FM
Anhydrous ethanol	64-17-5	SRC	None	>0.995	FM
Sodium hydroxide	1310-73-2	SRC	None	>0.960	FM
$[C_1OC_2mim][Ala]$	-	Synthesis	Solvent extraction, vacuum drying	>0.990	^1H, ^{13}C NMR
$[C_2OC_2mim][Ala]$	-	Synthesis	Solvent extraction, vacuum drying	>0.990	^1H, ^{13}C NMR

FM—Fractional melting; SRC—Shanghai Reagent Co., Ltd.

3.2. Preparation of ILs $[C_nOC_2mim][Ala](n = 1, 2)$

$[C_nOC_2mim][Ala](n = 1, 2)$ were prepared by Fukumoto's neutralization method [12], and $[C_nOC_2mim]Cl(n = 1, 2)$ by Sheldon's method [63]. An equal molar amount of 2-chloroethyl methyl ether or 2-chloroethyl ethyl ether was added dropwise to *N*-methylimidazole under nitrogen in a three-necked round-bottom flask while stirring at 298.15 K. The reaction temperature reached 353.15 K with 2-chloroethyl methyl ether and 373.15 K with 2-chloroethyl ethyl ether. The reactions lasted for 48 h and produced light yellow liquids, which were then washed three times with ethyl acetate, producing $[C_nOC_2mim]Cl(n = 1, 2)$. These were transformed into $[C_nOC_2mim]OH(n = 1, 2)$ using basic anion exchange resin conditioned with sodium hydroxide [29]. The aqueous $[C_nOC_2mim]OH(n = 1, 2)$ were then added dropwise (at slight excess) to aqueous DL-alanine and reacted for 72 h, yielding $[C_nOC_2mim][Ala](n = 1, 2)$. Water was removed by rotary evaporation and excess DL-alanine by ethanol:acetonitrile (9:1). The solvents were evaporated under reduced pressure and $[C_nOC_2mim][Ala](n = 1, 2)$ were dried in a vacuum oven for 60 h at 353.15 K. The chemical structures of $[C_nOC_2mim][Ala](n = 1, 2)$ are shown in Figure 6.

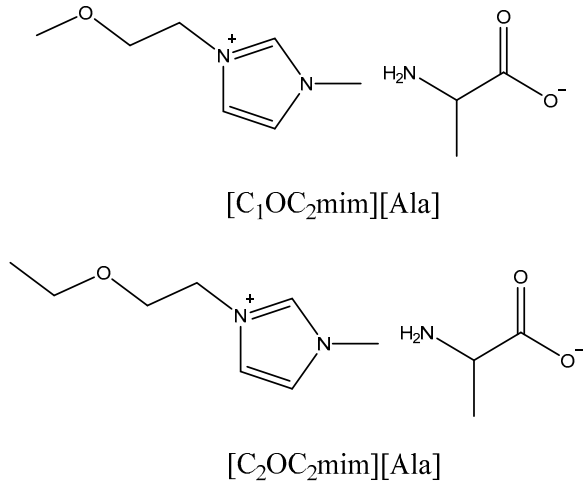

Figure 6. Chemical structures of ionic liquids [$C_n$$OC_2$mim][Ala]($n$ = 1, 2).

3.3. Analytical Methods

The structures of [$C_n$$OC_2$mim][Ala]($n$ = 1, 2) were characterized by NMR (Varian XL-300), as shown in the Supplementary Materials. The final water contents (w_2) of [$C_n$$OC_2$mim][Ala]($n$ = 1, 2), as measured using a ZSD-2 Karl Fischer moisture titrator, were 0.00472 and 0.00640 ± 0.0001 (mass fraction), respectively.

Since [$C_n$$OC_2$mim][Ala]($n$ = 1, 2) form strong hydrogen bonds with water, it is difficult to remove all traces of water from these ILs, which affects their density, surface tension, and refractive index. Therefore, the standard addition method was used to determine these properties. Each parameter was measured in [$C_n$$OC_2$mim][Ala]($n$ = 1, 2) at different water contents following heating at graduated temperatures. Values were then plotted against water content, and the intercept of the regression lines yielded the parameter values in the anhydrous ILs at a given temperature.

4. Conclusions

[$C_n$$OC_2$mim][Ala]($n$ = 1, 2) were prepared and their structures confirmed by NMR. Density, surface tension, and refractive index were determined by the standard addition method. Adding methylene to the aliphatic chain of an IL increased its standard entropy. Lattice energy and association enthalpy measurements showed that molecules of [$C_1$$OC_2$mim][Ala] were more compacted, and their intermolecular interactions stronger, than [$C_2$$OC_2$mim][Ala]. An improved Lorentz-Lorenz equation predicted the surface tension of both ionic and molecular liquids. A new compartmentalized polarity scale (P_N) based on molar surface Gibbs energy and dipole moments is presented. It encompasses the polarity of both the surface and body of a liquid. [$C_1$$OC_2$mim][Ala] is shown to have higher polarity than [$C_2$$OC_2$mim][Ala] based on P_N. The validity of P_N is demonstrated by comparison with alternative polarity scales and published polarities of both ionic and molecular liquids.

Supplementary Materials: The following supporting information can be downloaded at: https://www.mdpi.com/article/10.3390/molecules27103231/s1, Figure S1. ^{1}H NMR spectrum of IL [COC_2mim][Ala]; Figure S2. ^{1}H NMR spectrum of IL [$C_2$$OC_2$mim][Ala]; Figure S3. ^{13}C NMR spectrum of IL [COC_2mim][Ala]; Figure S4. ^{13}C NMR spectrum of IL [$C_2$$OC_2$mim][Ala]; Table S1. Densities of Ionic Liquids Containing Various Amounts of Water at pressure p = 0.1 MPa; Table S2. Surface Tensions of Ionic Liquids Containing Various Amounts of Water at pressure p = 0.1 MPa; Table S3. Refractive Indexes of Ionic Liquids Containing Various Amount of Water at pressure p = 0.1 MPa; Table S4. The values of molar volume, $V/\mathrm{cm}^3\cdot\mathrm{mol}^{-1}$ and molecular volume, V_m/nm^3 for the ILs [$C_n$$OC_2$mim][Ala]($n$ = 1, 2); Table S5. Molecular volume, V_m, standard molar entropy, S^0, lattice energy, U_{POT}, vaporization enthalpy, $\Delta_{lg}H_m{}^0$, association enthalpy, $\Delta_A H_m{}^0$ for some ionic liquids; Table S6. The estimated surface tension, $\gamma_{(est)}$, experimental surface tension, $\gamma_{(exp)}$,

refractive index, n_D, experimental density ρ(exp), molar surface Gibbs energy, g_s, molar refraction, R_m, molar volume, V for different ILs and molecular liquids; Table S7. The molar surface entropy, s, for some ILs; Density, ρ, surface tension, and refractive index, nD measuring methods; citation of ref. [30,39,43,52,54,55,64–106].

Author Contributions: Writing—original draft preparation, X.Z.; data curation, C.G.; visualization, W.W.; supervision, J.T. All authors have read and agreed to the published version of the manuscript.

Funding: This research was funded by National Natural Science Foundation of China, grant number 21773100; the Education Bureau of Liaoning Province, grant number LJC202005; and the Liaoning BaiQianWan Talents Program.

Institutional Review Board Statement: Not applicable.

Informed Consent Statement: Not applicable.

Data Availability Statement: Not applicable.

Conflicts of Interest: The authors declare no conflict of interest.

Sample Availability: Samples of compounds are available from the authors.

References

1. Blanchard, L.A.; Hancu, D.; Beckman, E.J.; Brennecke, J.F. Green processing using ionic liquids and CO_2. *Nature* **1999**, *399*, 28–29. [CrossRef]
2. Wei, G.-T.; Yang, Z.; Lee, C.-Y.; Yang, H.-Y.; Wang, C.C. Aqueous− organic phase transfer of gold nanoparticles and gold nanorods using an ionic liquid. *J. Am. Chem. Soc.* **2004**, *126*, 5036–5037. [CrossRef] [PubMed]
3. Kim, G.-T.; Jeong, S.; Xue, M.-Z.; Balducci, A.; Winter, M.; Passerini, S.; Alessandrini, F.; Appetecchi, G. Development of ionic liquid-based lithium battery prototypes. *J. Power Sources* **2012**, *199*, 239–246. [CrossRef]
4. Liu, Y.; Yao, X.; Yao, H.; Zhou, Q.; Xin, J.; Lu, X.; Zhang, S. Degradation of poly(ethylene terephthalate) catalyzed by metal-free choline-based ionic liquids. *Green Chem.* **2020**, *22*, 3122–3131. [CrossRef]
5. Williams, H.D.; Sahbaz, Y.; Ford, L.; Nguyen, T.-H.; Scammells, P.J.; Porter, C.J. Ionic liquids provide unique opportunities for oral drug delivery: Structure optimization and in vivo evidence of utility. *Chem. Commun.* **2014**, *50*, 1688–1690. [CrossRef]
6. Shamshina, J.L.; Kelley, S.P.; Gurau, G.; Rogers, R.D. Chemistry: Develop ionic liquid drugs. *Nat. News* **2015**, *528*, 188. [CrossRef]
7. Rahim, A.H.A.; Yunus, N.M.; Hamzah, W.S.W.; Sarwono, A.; Muhammad, N. Low-Viscosity Ether-Functionalized Ionic Liquids as Solvents for the Enhancement of Lignocellulosic Biomass Dissolution. *Processes* **2021**, *9*, 261. [CrossRef]
8. Zhang, S.; Li, J.; Jiang, N.; Li, X.; Pasupath, S.; Fang, Y.; Liu, Q.; Dang, D. Rational Design of an Ionic Liquid-Based Electrolyte with High Ionic Conductivity Towards Safe Lithium/Lithium-Ion Batteries. *Chem.—Asian J.* **2019**, *14*, 2810–2814. [CrossRef]
9. Zeng, S.; Wang, J.; Bai, L.; Wang, B.; Gao, H.; Shang, D.; Zhang, X.; Zhang, S. Highly selective capture of CO_2 by ether-functionalized pyridinium ionic liquids with low viscosity. *Energy Fuels* **2015**, *29*, 6039–6048. [CrossRef]
10. Trush, M.; Metelytsia, L.; Semenyuta, I.; Kalashnikova, L.; Papeykin, O.; Venger, I.; Tarasyuk, O.; Bodachivska, L.; Blagodatnyi, V.; Rogalsky, S. Reduced ecotoxicity and improved biodegradability of cationic biocides based on ester-functionalized pyridinium ionic liquids. *Environ. Sci. Pollut. Res.* **2019**, *26*, 4878–4889. [CrossRef]
11. Qu, Y.; Lan, J.; Chen, Y.; Sun, J. Amino acid ionic liquids as efficient catalysts for CO_2 capture and chemical conversion with epoxides under metal/halogen/cocatalyst/solvent-free conditions. *Sustain. Energy Fuels* **2021**, *5*, 2494–2503. [CrossRef]
12. Fukumoto, K.; Yoshizawa, M.; Ohno, H. Room temperature ionic liquids from 20 natural amino acids. *J. Am. Chem. Soc.* **2005**, *127*, 2398–2399. [CrossRef] [PubMed]
13. Yang, Z.; Sun, C.; Zhang, C.; Zhao, S.; Cai, M.; Liu, Z.; Yu, Q. Amino acid ionic liquids as anticorrosive and lubricating additives for water and their environmental impact. *Tribol. Int.* **2021**, *153*, 106663. [CrossRef]
14. Jiang, J.; Mu, X.; Qiao, J.; Su, Y.; Qi, L. New chiral ligand exchange capillary electrophoresis system with chiral amino amide ionic liquids as ligands. *Talanta* **2017**, *175*, 451–456. [CrossRef] [PubMed]
15. Tang, F.; Zhang, Q.; Ren, D.; Nie, Z.; Liu, Q.; Yao, S. Functional amino acid ionic liquids as solvent and selector in chiral extraction. *J. Chromatogr. A* **2010**, *1217*, 4669–4674. [CrossRef] [PubMed]
16. Ghavre, M.; Byrne, O.; Altes, L.; Surolia, P.K.; Spulak, M.; Quilty, B.; Thampi, K.R.; Gathergood, N. Low toxicity functionalised imidazolium salts for task specific ionic liquid electrolytes in dye-sensitised solar cells: A step towards less hazardous energy production. *Green Chem.* **2014**, *16*, 2252–2265. [CrossRef]
17. Kebaili, H.; Pérez de los Ríos, A.; Salar-García, M.J.; Ortiz-Martínez, V.M.; Kameche, M.; Hernández-Fernández, J.; Hernández-Fernández, F.J. Evaluating the toxicity of ionic liquids on Shewanella sp. for designing sustainable bioprocesses. *Front. Mater.* **2020**, *7*, 387. [CrossRef]
18. Jouyban, A.; Mirheydari, S.N.; Barzegar-Jalali, M.; Shekaari, H.; Acree, W.E. Comprehensive models for density prediction of ionic liquid+ molecular solvent mixtures at different temperatures. *Phys. Chem. Liq.* **2020**, *58*, 309–324. [CrossRef]

19. Chen, Z.; Huo, Y.; Cao, J.; Xu, L.; Zhang, S. Physicochemical Properties of Ether-Functionalized Ionic Liquids: Understanding Their Irregular Variations with the Ether Chain Length. *Ind. Eng. Chem. Res.* **2016**, *55*, 11589–11596. [CrossRef]
20. Pham, T.P.T.; Cho, C.-W.; Yun, Y.-S. Environmental fate and toxicity of ionic liquids: A review. *Water Res.* **2010**, *44*, 352–372. [CrossRef]
21. Atashrouz, S.; Amini, E.; Pazuki, G. Modeling of surface tension for ionic liquids using group method of data handling. *Ionics* **2015**, *21*, 1595–1603. [CrossRef]
22. Holbrey, J.D.; Rogers, R.D.; Mantz, R.A.; Trulove, P.C.; Cocalia, V.A.; Visser, A.E.; Anderson, J.L.; Anthony, J.L.; Brennecke, J.F.; Maginn, E.J.; et al. Physicochemical Properties. In *Ionic Liquids in Synthesis*; 2007; pp. 57–174. Available online: https://onlinelibrary.wiley.com/doi/book/10.1002/9783527621194 (accessed on 22 April 2022).
23. Nemec, T. Prediction of surface tension of binary mixtures with the parachor method. In *EPJ Web of Conferences*; EDP Sciences: Les Ulis, France, 2015; Volume 92, p. 02054.
24. Paduszynski, K. Extensive Databases and Group Contribution QSPRs of Ionic Liquid Properties. 3: Surface Tension. *Ind. Eng. Chem. Res.* **2021**, *60*, 5705–5720. [CrossRef]
25. Shukla, S.K.; Kumar, A. Polarity issues in room temperature ionic liquids. *Clean Technol. Environ. Policy* **2015**, *17*, 1111–1116. [CrossRef]
26. Cláudio, A.F.M.; Swift, L.; Hallett, J.P.; Welton, T.; Coutinho, J.A.P.; Freire, M.G. Extended scale for the hydrogen-bond basicity of ionic liquids. *Phys. Chem. Chem. Phys.* **2014**, *16*, 6593–6601. [CrossRef] [PubMed]
27. Kurnia, K.A.; Lima, F.; Cláudio, A.F.M.; Coutinho, J.A.P.; Freire, M.G. Hydrogen-bond acidity of ionic liquids: An extended scale. *Phys. Chem. Chem. Phys.* **2015**, *17*, 18980–18990. [CrossRef] [PubMed]
28. Hong, M.; Liu, R.J.; Yang, H.X.; Guan, W.; Tong, J.; Yang, J.Z. Determination of the vaporisation enthalpies and estimation of the polarity for 1-alkyl-3-methylimidazolium propionate {C(n)mim Pro (n = 2, 3)} ionic liquids. *J. Chem. Thermodyn.* **2014**, *70*, 214–218. [CrossRef]
29. Zheng, X.; Gong, Y.; Jiang, W.; Yu, K.; Tong, J.; Yang, J. The application of molar surface Gibbs energy to predicting ILs' properties. *J. Mol. Liq.* **2019**, *288*, 111004. [CrossRef]
30. Tong, J.; Hong, M.; Chen, Y.; Wang, H.; Guan, W.; Yang, J.-Z. The surface tension, density and refractive index of amino acid ionic liquids: C(3)mim Gly and C(4)mim Gly. *J. Chem. Thermodyn.* **2012**, *54*, 352–357. [CrossRef]
31. Singh, D.; Gardas, R.L. Influence of Cation Size on the Ionicity, Fluidity, and Physiochemical Properties of 1,2,4-Triazolium Based Ionic Liquids. *J. Phys. Chem. B* **2016**, *120*, 4834–4842. [CrossRef]
32. Glasser, L. Lattice and phase transition thermodynamics of ionic liquids. *Thermochim. Acta* **2004**, *421*, 87–93. [CrossRef]
33. Gusain, R.; Panda, S.; Bakshi, P.S.; Gardas, R.L.; Khatri, O.P. Thermophysical properties of trioctylalkylammonium bis(salicylato)borate ionic liquids: Effect of alkyl chain length. *J. Mol. Liq.* **2018**, *269*, 540–546. [CrossRef]
34. Lambert, F.L.; Leff, H.S. The Correlation of Standard Entropy with Enthalpy Supplied from 0 to 298.15 K. *J. Chem. Educ.* **2009**, *86*, 94–98. [CrossRef]
35. Tong, J.; Qu, Y.; Li, K.; Chen, T.-F.; Tong, J.; Yang, J.-Z. The molar surface Gibbs energy of the aqueous solution of the ionic liquid [C6mim][OAc]. *J. Chem. Thermodyn.* **2016**, *97*, 362–366. [CrossRef]
36. Myers, R.T. True molar surface energy and alignment of surface molecules. *J. Colloid Interface Sci.* **2004**, *274*, 229–236. [CrossRef] [PubMed]
37. Ersfeld, B.; Felderhof, B.U. Retardation correction to the Lorentz-Lorenz formula for the refractive index of a disordered system of polarizable point dipoles. *Phys. Rev. E* **1998**, *57*, 1118–1126. [CrossRef]
38. Zhang, D.; Jiang, W.; Liu, L.; Yu, K.; Hong, M.; Tong, J. The molar surface Gibbs energy and polarity of ether-functionalized ionic liquids. *J. Chem. Thermodyn.* **2019**, *138*, 313–320. [CrossRef]
39. Hong, M.; Sun, A.; Liu, C.; Guan, W.; Tong, J.; Yang, J.-Z. Physico-Chemical Properties of 1-Alkyl-3-methylimidazolium Propionate Ionic Liquids {[Cnmim][Pro](n = 3, 4, 5, 6)} from 288.15 K to 328.15 K. *Ind. Eng. Chem. Res.* **2013**, *52*, 15679–15683. [CrossRef]
40. Seoane, R.G.; Corderí, S.; Gómez, E.; Calvar, N.; González, E.J.; Macedo, E.A.; Domínguez, Á. Temperature Dependence and Structural Influence on the Thermophysical Properties of Eleven Commercial Ionic Liquids. *Ind. Eng. Chem. Res.* **2012**, *51*, 2492–2504. [CrossRef]
41. Sun, Q.; Yang, W.; Cheng, Y.; Dong, J.; Zhu, M.; Zhang, B.; Dubois, A.; Zhu, M.; Jie, W.; Xu, Y. Anisotropic dielectric behavior of layered perovskite-like Cs3Bi2I9 crystals in the terahertz region. *Phys. Chem. Chem. Phys.* **2020**, *22*, 24555–24560. [CrossRef]
42. Weiß, N.; Schmidt, C.H.; Thielemann, G.; Heid, E.; Schröder, C.; Spange, S. The physical significance of the Kamlet–Taft π* parameter of ionic liquids. *Phys. Chem. Chem. Phys.* **2021**, *23*, 1616–1626. [CrossRef]
43. Wei, J.; Fan, B.-H.; Pan, Y.; Xing, N.-N.; Men, S.-Q.; Tong, J.; Guan, W. Vaporization enthalpy and the molar surface Gibbs free energy for ionic liquids C(n)Dmim NTF2 (n = 2, 4). *J. Chem. Thermodyn.* **2016**, *101*, 278–284. [CrossRef]
44. Peter Atkins, P.; De Paula, J. *Atkins' Physical Chemistry*; OUP Oxford: Oxford, UK, 2014.
45. Zhang, D.; Li, B.; Hong, M.; Kong, Y.-X.; Tong, J.; Xu, W.-G. Synthesis and characterization of physicochemical properties of new ether-functionalized amino acid ionic liquids. *J. Mol. Liq.* **2020**, *304*, 112718. [CrossRef]
46. Zhao, Y.; Lv, J.; Liu, H.; Wu, J.; Tong, J. Study on the polarity and molar surface Gibbs energy of ether-based amino acid ionic liquids [COC4mim][Gly], [COC4mim][Ala] and [COC4mim][Thr]. *J. Mol. Liq.* **2021**, *336*, 116094. [CrossRef]
47. Hildebrand, J.H.; Scott, R.L. *The Solubility of Nonelectrolytes*; Reinhold Publishing Corporation: New York, NY, USA; London Chapman and Hall: London, UK, 1950.

48. Lawson, D.D.; Ingham, J. Estimation of solubility parameters from refractive index data. *Nature* **1969**, *223*, 614. [CrossRef]
49. Deetlefs, M.; Seddon, K.R.; Shara, M. Predicting physical properties of ionic liquids. *Phys. Chem. Chem. Phys.* **2006**, *8*, 642–649. [CrossRef]
50. Masaki, T.; Nishikawa, K.; Shirota, H. Microscopic Study of Ionic Liquid− H_2O Systems: Alkyl-Group Dependence of 1-Alkyl-3-Methylimidazolium Cation. *J. Phys. Chem. B* **2010**, *114*, 6323–6331. [CrossRef]
51. Chen, Y.; Sun, Y.; Li, Z.; Wang, R.; Hou, A.; Yang, F. Volumetric properties of binary mixtures of ionic liquid with tributyl phosphate and dimethyl carbonate. *J. Chem. Thermodyn.* **2018**, *123*, 165–173. [CrossRef]
52. Verevkin, S.P.; Zaitsau, D.H.; Emel'yanenko, V.N.; Yermalayeu, A.V.; Schick, C.; Liu, H.; Maginn, E.J.; Bulut, S.; Krossing, I.; Kalb, R. Making sense of enthalpy of vaporization trends for ionic liquids: New experimental and simulation data show a simple linear relationship and help reconcile previous data. *J. Phys. Chem. B* **2013**, *117*, 6473–6486. [CrossRef]
53. Li, Z.; Sun, Y.; Zhao, D.; Zhuang, Y.; Wang, R.; Yang, F.; Liu, X.; Chen, Y. Surface tension of binary mixtures of (ionic liquid+ tributyl phosphate). *J. Chem. Thermodyn.* **2019**, *132*, 214–221. [CrossRef]
54. Luo, H.; Baker, G.A.; Dai, S. Isothermogravimetric determination of the enthalpies of vaporization of 1-alkyl-3-methylimidazolium ionic liquids. *J. Phys. Chem. B* **2008**, *112*, 10077–10081. [CrossRef]
55. Xu, W.-G.; Li, L.; Ma, X.-X.; Wei, J.; Duan, W.-B.; Guan, W.; Yang, J.-Z. Density, surface tension, and refractive index of ionic liquids homologue of 1-alkyl-3-methylimidazolium tetrafluoroborate [C n mim][BF4](n = 2, 3, 4, 5, 6). *J. Chem. Eng. Data* **2012**, *57*, 2177–2184. [CrossRef]
56. Tao, G.-H.; Zou, M.; Wang, X.-H.; Chen, Z.-Y.; Evans, D.; Kou, Y. Comparison of Polarities of Room-Temperature Ionic Liquids Using FT-IR Spectroscopic Probes. *Aust. J. Chem.—AUST J CHEM* **2005**, *58*, 327–331. [CrossRef]
57. Park, S.; Kazlauskas, R.J. Improved Preparation and Use of Room-Temperature Ionic Liquids in Lipase-Catalyzed Enantio- and Regioselective Acylations. *J. Org. Chem.* **2001**, *66*, 8395–8401. [CrossRef] [PubMed]
58. Wu, Y.; Sasaki, T.; Kazushi, K.; Seo, T.; Sakurai, K. Interactions between Spiropyrans and Room-Temperature Ionic Liquids: Photochromism and Solvatochromism. *J. Phys. Chem. B* **2008**, *112*, 7530–7536. [CrossRef] [PubMed]
59. Lide, D.R. *CRC Handbook of Chemistry and Physics*; CRC Press: Boca Raton, FL, USA, 2004; Volume 85.
60. Potangale, M.; Tiwari, S. Correlation of the empirical polarity parameters of solvate ionic liquids (SILs) with molecular structure. *J. Mol. Liq.* **2020**, *297*, 111882. [CrossRef]
61. Spange, S.; Lienert, C.; Friebe, N.; Schreiter, K. Complementary interpretation of ET (30) polarity parameters of ionic liquids. *Phys. Chem. Chem. Phys.* **2020**, *22*, 9954–9966. [CrossRef]
62. Tong, J.; Zheng, X.; Li, H.; Tong, J.; Liu, Q. Densities and Viscosities of Aqueous Amino Acid Ionic Liquids [Cnmim][Ala](n = 3, 4, 5). *J. Chem. Eng. Data* **2017**, *62*, 2501–2508. [CrossRef]
63. Liu, Q.; Janssen, M.H.; van Rantwijk, F.; Sheldon, R.A. Room-temperature ionic liquids that dissolve carbohydrates in high concentrations. *Green Chem.* **2005**, *7*, 39–42. [CrossRef]
64. Ma, X.-X.; Wei, J.; Zhang, Q.-B.; Tian, F.; Feng, Y.-Y.; Guan, W. Prediction of Thermophysical Properties of Acetate-Based Ionic Liquids Using Semiempirical Methods. *Ind. Eng. Chem. Res.* **2013**, *52*, 9490–9496. [CrossRef]
65. Wei, J.; Bu, X.; Guan, W.; Xing, N.; Fang, D.; Wu, Y. Measurement of vaporization enthalpy by isothermogravimetrical method and prediction of the polarity for 1-alkyl-3-methylimidazolium acetate {[C n mim][OAc](n= 4, 6)} ionic liquids. *RSC Adv.* **2015**, *5*, 70333–70338. [CrossRef]
66. Tong, J.; Yang, H.X.; Liu, R.J.; Li, C.; Xia, L.X.; Yang, J.Z. Determination of the Enthalpy of Vaporization and Prediction of Surface Tension for Ionic Liquid 1-Alkyl-3-methylimidazolium Propionate C(n)mim Pro (n=4, 5, 6). *J. Phys. Chem. B* **2014**, *118*, 12972–12978. [CrossRef] [PubMed]
67. Tong, J.; Hong, M.; Liu, C.; Sun, A.; Guan, W.; Yang, J.-Z. Estimation of Properties of Ionic Liquids 1-Alkyl-3-methylimidazolium Lactate Using a Semiempirical Method. *Ind. Eng. Chem. Res.* **2013**, *52*, 4967–4972. [CrossRef]
68. Wei, J.; Li, Z.; Gu, C.; Pan, Y.; Xing, N.-N.; Tong, J.; Guan, W. Determination of vaporization enthalpy for ionic liquids C(n)mim Lact (n=2, 3, 5) and applications of the molar surface Gibbs free energy. *J. Therm. Anal. Calorim.* **2016**, *125*, 547–556. [CrossRef]
69. Wei, J.; Ma, T.; Ma, X.; Guan, W.; Liu, Q.; Yang, J. Study on thermodynamic properties and estimation of polarity of ionic liquids { C(n)mmim NTf2 (n=2, 4)}. *Rsc Adv.* **2014**, *4*, 30725–30732. [CrossRef]
70. Verevkin, S.P. Predicting enthalpy of vaporization of ionic liquids: A simple rule for a complex property. *Angew. Chem.-Int. Ed.* **2008**, *47*, 5071–5074. [CrossRef]
71. Hong, M.; Sun, A.; Yang, Q.; Guan, W.; Tong, J.; Yang, J.-Z. Studies on properties of ionic liquids 1-alkyl-3-methylimidazolium lactate at temperatures from (288.15 to 333.15)K. *J. Chem. Thermodyn.* **2013**, *67*, 91–98. [CrossRef]
72. Fang, D.-W.; Tong, J.; Guan, W.; Wang, H.; Yang, J.-Z. Predicting Properties of Amino Acid Ionic Liquid Homologue of 1-Alkyl-3-methylimidazolium Glycine. *J. Phys. Chem. B* **2010**, *114*, 13808–13814. [CrossRef]
73. Wei, J.; Chang, C.; Zhang, Y.; Hou, S.; Fang, D.; Guan, W. Prediction of thermophysical properties of novel ionic liquids based on serine C(n)mim Ser (n=3,4) using semiempirical methods. *J. Chem. Thermodyn.* **2015**, *90*, 310–316. [CrossRef]
74. Clara, R.A.; Marigliano, A.C.G.; Solimo, H.N. Density, viscosity, isothermal (vapour plus liquid) equilibrium, excess molar volume, viscosity deviation, and their correlations for chloroform plus methyl isobutyl ketone binary system. *J. Chem. Thermodyn.* **2007**, *39*, 261–267. [CrossRef]
75. Dragoescu, D. Refractive indices and their related properties for several binary mixtures containing cyclic ketones and chloroalkanes. *J. Mol. Liq.* **2015**, *209*, 713–722. [CrossRef]

76. Fenclová, D.; Vrbka, P.; Dohnal, V.; Řehák, K.; García-Miaja, G. (Vapour + liquid) equilibria and excess molar enthalpies for mixtures with strong complex formation. Trichloromethane or 1-bromo-1-chloro-2,2,2-trifluoroethane (halothane) with tetrahydropyran or piperidine. *J. Chem. Thermodyn.* **2002**, *34*, 361–376. [CrossRef]
77. Helm, R.V.; Lanum, W.J.; Cook, G.L.; Ball, J.S. Purification and Properties of Pyrrole, Pyrrolidine, Pyridine and 2-Methylpyridine. *J. Phys. Chem.* **1958**, *62*, 858–862. [CrossRef]
78. Lagemann, R.T.; McMillan, D.R., Jr.; Woolf, W.E. Temperature Variation of Ultrasonic Velocity in Liquids. *J. Chem. Phys.* **1949**, *17*, 369–373. [CrossRef]
79. Colnay, M.E.; Vasseur, A.; Guerin, M. The influence of non-polar solvents on molecular dielectric polarization. 1: An attempt to select by experiment appropriate expressions. *J. Chem. Res* **1983**, *9*, 220–221.
80. Gill, D.S.; Singh, P.; Singh, J.; Singh, P.; Senanayake, G.; Hefter, G.T. Ultrasonic velocity, conductivity, viscosity and calorimetric studies of copper(i) and sodium perchlorates in cyanobenzene, pyridine and cyanomethane. *J. Chem. Soc.-Faraday Trans.* **1995**, *91*, 2789–2795. [CrossRef]
81. Sharma, B.R.; Singh, P.P. Excess Gibbs energies of mixing for some binary mixtures. *J. Chem. Eng. Data* **1975**, *20*, 360–363. [CrossRef]
82. Kyte, C.; Jeffery, G.; Vogel, A. 864. Physical properties and chemical constitution. Part XXVIII. Pyridine derivatives. *J. Chem. Soc. (Resumed)* **1960**, 4454–4472. [CrossRef]
83. Ortega, J. Densities and refractive-indexes of pure alcohols as a function of temperature. *J. Chem. Eng. Data* **1982**, *27*, 312–317. [CrossRef]
84. Vijande, J.; Piñeiro, M.M.; García, J.; Valencia, A.J.L.; Legido, J.L. Density and Surface Tension Variation with Temperature for Heptane + 1-Alkanol. *J. Chem. Eng. Data* **2006**, *51*, 1778–1782. [CrossRef]
85. Das, K.N.; Habibullah, M.; Rahman, I.M.M.; Hasegawa, H.; Uddin, M.A.; Saifuddin, K. Thermodynamic Properties of the Binary Mixture of Hexan-1-ol with m-Xylene at T = (303.15, 313.15, and 323.15) K. *J. Chem. Eng. Data* **2009**, *54*, 3300–3302. [CrossRef]
86. Neyband, R.S.; Yousefi, A.; Zarei, H. Experimental and Computational Thermodynamic Properties of (Benzyl Alcohol plus Alkanols) Mixtures. *J. Chem. Eng. Data* **2015**, *60*, 2291–2300. [CrossRef]
87. Venkatramana, L.; Sivakumar, K.; Gardas, R.; Reddy, K.D. Effect of chain length of alcohol on thermodynamic properties of their binary mixtures with benzylalcohol. *Thermochim. Acta* **2014**, *581*, 123–132. [CrossRef]
88. Weissler, A. Ultrasonic Investigation of Molecular Properties of Liquids. II. [1] The Alcohols[1a]. *J. Am. Chem. Soc.* **1948**, *70*, 1634–1640. [CrossRef] [PubMed]
89. Huang, T.-T.; Yeh, C.-T.; Tu, C.-H. Densities, Viscosities, Refractive Indices, and Surface Tensions for the Ternary Mixtures of 2-Propanol + Benzyl Alcohol + 2-Phenylethanol at T = 308.15 K. *J. Chem. Eng. Data* **2008**, *53*, 1203–1207. [CrossRef]
90. Hiers, G.S.; Adams, R. Omega-cyclohexyl derivatives of various normal aliphatic acids. IV. *J. Am. Chem. Soc.* **1926**, *48*, 2385–2393. [CrossRef]
91. Hovorka, S.; Roux, A.H.; Roux-Desgranges, G.; Dohnal, V. Limiting partial molar excess heat capacities and volumes of selected organic compounds in water at 25 degrees C. *J. Solut. Chem.* **1999**, *28*, 1289–1305. [CrossRef]
92. Shinomiya, T. Dielectric Relaxation and Intermolecular Association of Alicyclic Alcohols in Liquid and Solid States. *Bull. Chem. Soc. Jpn.* **1990**, *63*, 1087–1092. [CrossRef]
93. Lasich, M.; Moodley, T.; Bhownath, R.; Naidoo, P.; Ramjugernath, D. Liquid–Liquid Equilibria of Methanol, Ethanol, and Propan-2-ol with Water and Dodecane. *J. Chem. Eng. Data* **2011**, *56*, 4139–4146. [CrossRef]
94. Zarei, H.A.; Shahvarpour, S. Volumetric Properties of Binary and Ternary Liquid Mixtures of 1-Propanol (1) + 2-Propanol (2) + Water (3) at Different Temperatures and Ambient Pressure (81.5 kPa). *J. Chem. Eng. Data* **2008**, *53*, 1660–1668. [CrossRef]
95. Ashcroft, S.J.; Clayton, A.D.; Shearn, R.B. Isothermal vapor-liquid equilibriums for the systems toluene-n-heptane, toluene-propan-2-ol, toluene-sulfolane, and propan-2-ol-sulfolane. *J. Chem. Eng. Data* **1979**, *24*, 195–199. [CrossRef]
96. Ritzoulis, G. Excess properties of the binary liquid systems dimethylsulfoxide + isopropanol and propylene carbonate + isopropanol. *Can. J. Chem.* **1989**, *67*, 1105–1108. [CrossRef]
97. Almasi, M. Densities and viscosities of binary mixtures of ethylmethylketone and 2-alkanols; application of the ERAS model and cubic EOS. *Thermochim. Acta* **2013**, *554*, 25–31. [CrossRef]
98. Ruostesuo, P.; Pirilahonkanen, P. Thermodynamic and spectroscopic properties of 2-pyrrolidinones. 2. Dielectric-Properties of 2-pyrrolidinone in binary-mixtures. *J. Solut. Chem.* **1990**, *19*, 473–482. [CrossRef]
99. Olivieri, G.V.; da Cunha, C.S.; dos Santos Martins, L.; Paegle, P.A.M.; Nuncio, S.D.; de Araújo Morandim-Giannetti, A.; Torres, R.B. Thermodynamic and spectroscopic study of binary mixtures of n-butylammonium oleate ionic liquid plus alcohol at T=288.15-308.15 K. *J. Therm. Anal. Calorim.* **2018**, *131*, 2925–2942. [CrossRef]
100. Rafiee, H.R.; Frouzesh, F.; Miri, S. Volumetric properties for binary mixtures of ethyl acetate, vinyl acetate and tert-butyl acetate with 1-propanol and iso-butanol at T = (293.15–313.15) K and P=0.087 MPa. *J. Mol. Liq.* **2016**, *213*, 255–267. [CrossRef]
101. Zaoui-Djelloul-Daouadji, M.; Mokbel, I.; Bahadur, I.; Negadi, A.; Jose, J.; Ramjugernath, D.; Ebenso, E.E.; Negadi, L. Vapor-liquid equilibria, density and sound velocity measurements of (water or methanol or ethanol+1,3-propanediol) binary systems at different temperatures. *Thermochim. Acta* **2016**, *642*, 111–123. [CrossRef]
102. Vasanthakumar, A.; Bahadur, I.; Redhi, G.G.; Gengan, R.M.; Anand, K. Synthesis, characterization and thermophysical properties of ionic liquid N-methyl-N-(2′,3′-epoxypropyl)-2-oxopyrrolidinium chloride and its binary mixtures with water or ethanol at different temperatures. *J. Mol. Liq.* **2016**, *219*, 685–693. [CrossRef]

103. Yao, H.; Zhang, S.; Wang, J.; Zhou, Q.; Dong, H.; Zhang, X. Densities and Viscosities of the Binary Mixtures of 1-Ethyl-3-methylimidazolium Bis(trifluoromethylsulfonyl)imide with N-Methyl-2-pyrrolidone or Ethanol at T = (293.15 to 323.15) K. *J. Chem. Eng. Data* **2012**, *57*, 875–881. [CrossRef]
104. Yan, J.-H.; Dai, L.-Y.; Wang, X.-Z.; Chen, Y.-Q. Densities and Viscosities of Binary Mixtures of Cyclopropanecarboxylic Acid with Methanol, Ethanol, Propan-1-ol, and Butan-1-ol at Different Temperatures. *J. Chem. Eng. Data* **2009**, *54*, 1147–1152. [CrossRef]
105. Zarei, H.A.; Mirhidari, N.; Zangeneh, Z. Densities, Excess Molar Volumes, Viscosity, and Refractive Indices of Binary and Ternary Liquid Mixtures of Methanol (1) + Ethanol (2) + 1,2-Propanediol (3) at P = 81.5 kPa. *J. Chem. Eng. Data* **2009**, *54*, 847–854. [CrossRef]
106. Fan, W.; Zhou, Q.; Zhang, S.; Yan, R. Excess molar volume and viscosity deviation for the methanol plus methyl methacrylate binary system at T = (283.15 to 333.15) K. *J. Chem. Eng. Data* **2008**, *53*, 1836–1840. [CrossRef]